

Resistivity Structure of the Hiyoriyama Cryptodome at Kuttara Volcano, Hokkaido, Japan

Yoshihiko GOTO* and Akira JOHMORI**

(Received March 1, 2012; Accepted March 15, 2013)

Direct current (DC) electrical and controlled source audio-frequency magnetotelluric (CSAMT) surveys were performed over the Hiyoriyama Cryptodome in Kuttara Volcano, Hokkaido, Japan. Both surveys were performed on the same survey line across the cryptodome in a NE-SW orientation. Two-dimensional joint inversion of the DC electrical and CSAMT data revealed the underground resistivity structure at depths less than 400 m beneath the cryptodome. The resistivity structure suggests that the cryptodome comprises a dacite intrusion of 150 m wide and 80 m thick ($20\text{--}50 \Omega \cdot \text{m}$), and overlying pyroclastic deposits that are 10–30 m thick ($>100 \Omega \cdot \text{m}$). The dacite intrusion is underlain by a convex-shaped, low-resistivity layer ($<5 \Omega \cdot \text{m}$) that is interpreted to be smectite-rich, altered pyroclastic deposits that have been subjected to low-temperature ($<200^\circ\text{C}$) hydrothermal alteration. The low-resistivity layer is underlain by a slightly higher-resistivity layer ($10\text{--}30 \Omega \cdot \text{m}$) that is interpreted to be altered pyroclastic deposits that were subjected to higher-temperature ($>200^\circ\text{C}$) hydrothermal alteration in a relatively deep, hot region near the conduit of the cryptodome.

Key words: resistivity structure, DC electrical method, CSAMT method, Hiyoriyama Cryptodome, Kuttara Volcano

1. Introduction

Resistivity surveying provides valuable information on the underground geological structures of active volcanoes (e.g., Risk *et al.*, 2003; Aizawa *et al.*, 2008; Srigutomo *et al.*, 2008). We performed direct current (DC) electrical (for details of the method, see Milsom, 2003) and controlled source audio-frequency magnetotelluric (CSAMT) surveys (see Sandberg and Hohman, 1982) at the Hiyoriyama Cryptodome in Kuttara Volcano, southwestern Hokkaido, Japan, in order to investigate its internal structure. The cryptodome is inferred to have formed by the uplift of pre-existing pyroclastic deposits due to the intrusion of dacitic magma (Katsui *et al.*, 1988), but its internal structures are poorly constrained. This paper presents the results of the resistivity surveys and discusses the nature of subsurface geological structures beneath the cryptodome.

2. Hiyoriyama Cryptodome

The Hiyoriyama Cryptodome is located in the northern area of the Noboribetsu Geothermal Field, in the western part of Kuttara Volcano (Fig. 1). The volcano consists mainly of an andesitic stratovolcano (summit at 549 m above sea level) with a small caldera at the summit (Lake Kuttara). The volcano evolved over the period 80–45 ka, involving early silicic explosive activity and subsequent

stratovolcano building associated with caldera collapse at 40 ka (Katsui *et al.*, 1988; Yamagata, 1994; Moriizumi, 1998; Moriya, 2003).

The Noboribetsu Geothermal Field, which is inferred to have formed after the collapse of the caldera (Katsui *et al.*, 1988), is approximately 1 km wide (NE-SW) and 1.5 km long (NW-SE) (Fig. 1). The geology of the Noboribetsu Geothermal Field consists mainly of pyroclastic deposits erupted from Kuttara Volcano (mainly the Kt-1 pyroclastic flow deposit; Moriizumi, 1998). The deposits are >200 m thick (NEDO, 1991) and consist of dacitic pumice clasts up to tens of centimeters in diameter.

The Hiyoriyama Cryptodome (Fig. 2) is elliptical in plan view, ranging in diameter from 350 m (NE-SW) to 550 m (NW-SE). In cross-section, it has a pyramidal form with steeply sloping sides (Fig. 2A). It rises 130 m above the surrounding area, with the highest point being 377 m above sea level. The surface of the cryptodome is covered with pyroclastic deposits (<15 m thick) that were uplifted by growth of the dome (Katsui *et al.*, 1988). The cryptodome has an explosion crater (Hiyoriyama Summit Crater; Fig. 2B) at its summit. The crater is 40×95 m in area (elongate along a NW-SE axis) and 20 m deep, and contains active fumaroles (Goto *et al.*, 2011a, b) with a maximum temperature of 134°C (measured on 6 July 2009). The slopes of the

*College of Environmental Technology, Graduate School of Engineering, Muroran Institute of Technology, Mizumoto-cho 27-1, Muroran, Hokkaido 050-8585, Japan.

**Neo Science Co., Ltd., Tarui 4-2-30, Sennan, Osaka

590-0521, Japan.

Corresponding author: Yoshihiko Goto
e-mail: ygoto@mmm.muroran-it.ac.jp

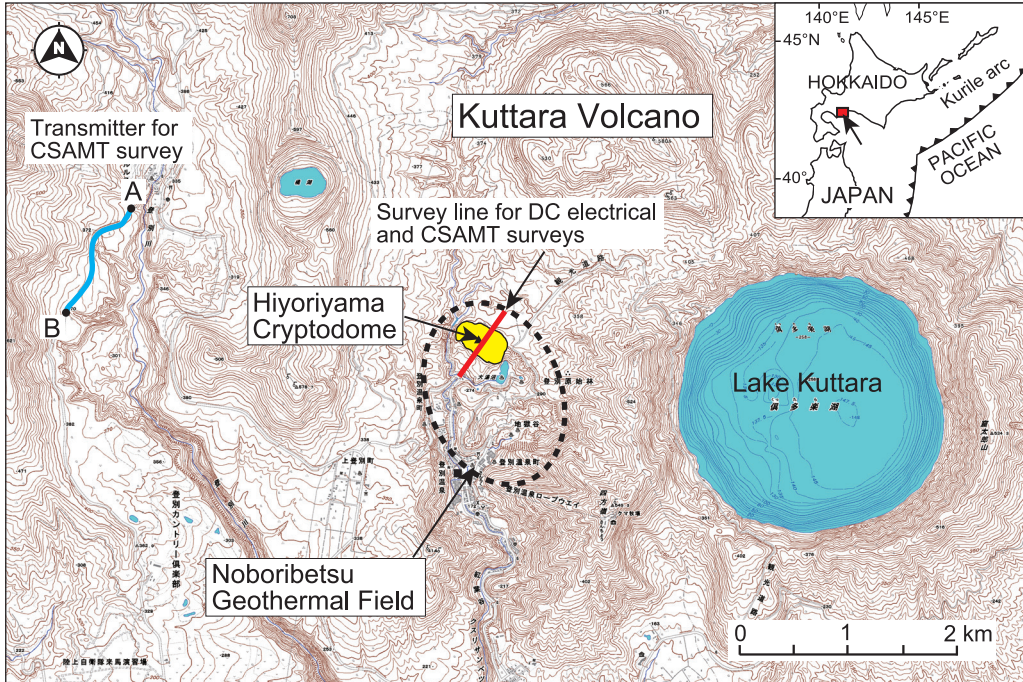


Fig. 1. Location map of the Hiyoriyama Cryptodome (yellow area) in the Noboribetsu Geothermal Field, lying in the western part of Kuttara Volcano, southwestern Hokkaido, Japan. Also shown is the location of the survey line for the DC electrical and CSAMT surveys (red line). The points marked A and B are the ends of the grounded-wire (dipole source) of the transmitter for the CSAMT survey (blue line). Topographic contour interval is 10 m.

cryptodome are widely covered with dense vegetation, apart from the southeastern slope that has been severely eroded by past phreatic eruptions from Oyunuma Lake (Fig. 2A). Fission-track dating indicates that the cryptodome formed at *ca.* 15 ka (Goto and Danhara, 2011).

The dacite intrusion beneath the Hiyoriyama Cryptodome is exposed on the wall of the Hiyoriyama Summit Crater, and is massive with columnar joints spaced at intervals of 1.0–1.5 m. The dacite is generally hydrothermally altered, although fresh dacite occurs sporadically at the crater rim. The fresh dacite is grey and porphyritic, containing phenocrysts of plagioclase, quartz, hypersthene, and trace amounts of augite, opaque minerals, and hornblende. The groundmass is granophytic, containing silica minerals, feldspars, and opaque minerals.

Geomorphological studies (Goto *et al.*, 2011a) suggest that the growth of the Hiyoriyama Cryptodome caused damming of a river and the deposition of sediments behind the dam, resulting in the formation of a plain to the northeast of the dome (Hiyoriyama Plain; Fig. 2B). The Hiyoriyama Plain is semi-rectangular in plan view, being 300 m (NW–SE) × 800 m (NE–SW) in size, and is covered by short bamboo and grasses. Drilling of the Hiyoriyama Plain (unpublished data) has revealed a 15-m-thick layer of peat underlain by fresh pyroclastic deposits (>6 m thick).

3. Resistivity surveys

The DC and CSAMT surveys were performed to obtain a continuous resistivity structure at depths of up to 400 m beneath the Hiyoriyama Cryptodome. The two surveys were performed on the same survey line, which crosses the Hiyoriyama Cryptodome in a NE–SW orientation (Figs. 2B and 3). Given that the cryptodome is elongated in a NW–SE orientation (Fig. 3), the feeder dyke that is the magma conduit beneath the dome is inferred to strike NW–SE (Goto *et al.*, 2011a). The NW–SE-trending feeder dyke probably occurs below the summit of the cryptodome (location M6 in Fig. 3). The survey line was oriented in such a way as to obtain a resistivity section perpendicular to the inferred feeder dyke.

3-1 DC electrical survey

The DC electrical survey was performed using the ‘high-density electrical prospecting’ method (Matsuoka, 2005), which employs a number of electrodes that are laid out on the ground surface in an array. In this method, a transmitter injects electrical currents to a pair of current electrodes, and the electric potential is measured using a pair of potential electrodes. The distance between the current electrodes and the potential electrodes dictates the depth of measurement. The resistivity structure is usually obtained by two-dimensional (2D) inversion using the

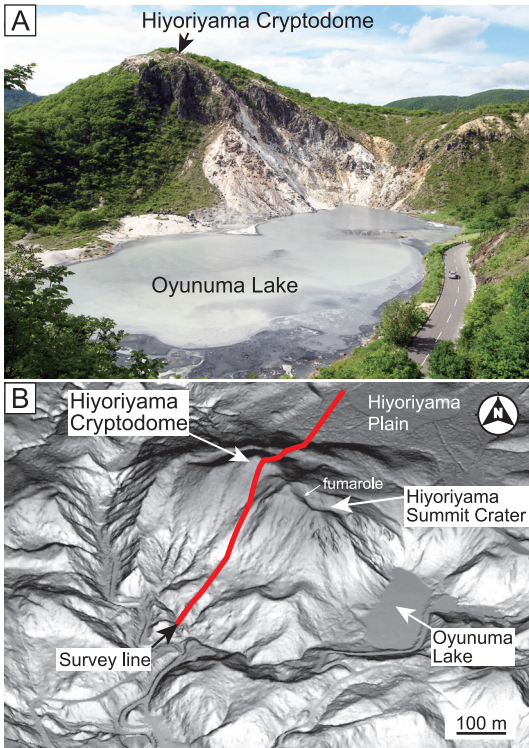


Fig. 2. (A) Photograph of the Hiyoriyama Cryptodome viewed from the south. (B) Oblique, three-dimensional, digital terrain model (DTM) of the Hiyoriyama Cryptodome viewed from the south (after Goto *et al.*, 2011a), showing the survey line for the DC electrical and CSAMT surveys (red line).

finite element method.

The DC electrical survey was carried out using a high-resolution electrical exploration system consisting of a transmitter-logger unit (McOHM Model-2115; Oyo Corporation), a switching box, take-out cables, and electrodes (Fig. 4A). The transmitter-logger unit comprises a transmitter with 400 Vp-p output voltage and a data logger with resolution of 20 μ V, powered by a 12 V car battery. The electrodes were connected to the transmitter-logger unit via the switching box and take-out cables. The specifications of the electrical survey system are listed in Table 1.

The survey line was 700 m long and oriented N35° E, passing over the summit of the Hiyoriyama Cryptodome (Fig. 3). The electrode configurations used were the Wenner and Eltran arrays (Fig. 4B), both of which are characterized by regular intervals of electrodes. We employed these arrays because the Wenner array is sensitive to horizontal structures, whereas the Eltran array is sensitive to vertical structures. The electrodes were set on the survey line at regular intervals of 10 m in the horizontal, using a transit and Global Positioning System (GPS). The number of

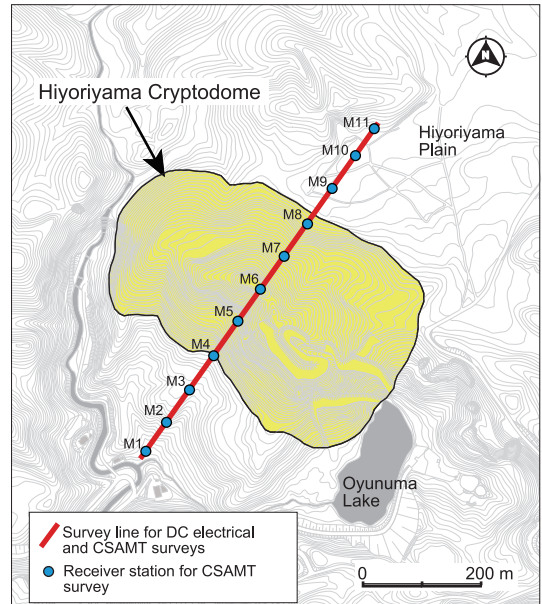


Fig. 3. Topographic map of the Hiyoriyama Cryptodome, showing the survey line for the DC electrical and CSAMT surveys (red line). Receiver stations (blue circles; M1–M11) for the CSAMT survey are also shown. The survey line is 700 m long and oriented N35° E, passing over the summit of the cryptodome. Receiver station M6 is located at the summit of the cryptodome.

electrodes was 71.

Measurements were carried out from 20 to 21 May 2011 (Fig. 5). During the measurements, two current electrodes (C1 and C2 in Fig. 4B) and two potential electrodes (P1 and P2 in Fig. 4B) were selected from the 71 electrodes. The transmitter-logger unit injected 20–50 mA electrical currents into the current electrodes, while electric potential was measured at the potential electrodes. A total of 1610 datasets were obtained by changing the sites and intervals of measuring electrodes using the switching box (Fig. 5). The distances between the measuring electrodes ranged from 10 to 230 m.

3-2 CSAMT survey

The CSAMT survey was performed following the ‘scalar CSAMT’ method (Matsuoka, 2005), whereby a transmitter injects electrical currents into the ground at audio (and near-audio) frequencies via a grounded-wire (dipole source), while a receiver records the electric field parallel to the grounded-wire and records the magnetic field perpendicular to the grounded-wire. The resistivity structure is usually obtained by 2D inversion using the finite element method, based on magnetotelluric (MT) theory.

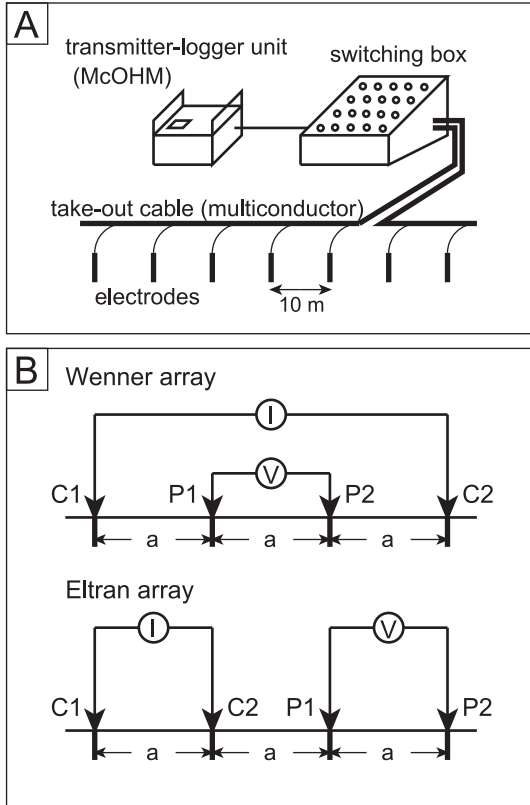


Fig. 4. (A) Schematic of the electrical exploration system used for the DC electrical survey. The system consists of a transmitter-logger unit (McOHM), a switching box, take-out cables (multiconductor cables), and 71 electrodes connected to the take-out cables. (B) Schematic of the electrode configuration (Wenner and Eltran arrays) used for the DC electrical survey. C1 and C2 are current electrodes; P1 and P2 are potential electrodes. V is the voltage difference between P1 and P2 due to a current (I) flowing between C1 and C2.

The CSAMT survey was carried out using a high-resolution electromagnetic system (Geo-SEM; Neuroscience Co. Ltd) consisting of a transmitter and a receiver, both of which are synchronized by GPS (Fig. 6). The transmitter (Fig. 7A) consists of a transformer, a rectifier, a switching circuit, a GPS clock, and a generator. A grounded-wire, 1.1 km long with 30 electrodes at each termination, was connected to the transmitter (Fig. 6). The receiver (Fig. 7B) consisted of an amplifier, a filter, a data logger, a GPS clock, and sensors. The sensors consist of a pair of electrodes and a coil. The transmitter and receiver were synchronized by a high-precision quartz clock system using GPS with an accuracy of 1×10^{-6} sec. The specifications of the Geo-SEM system are listed in Table 1, and

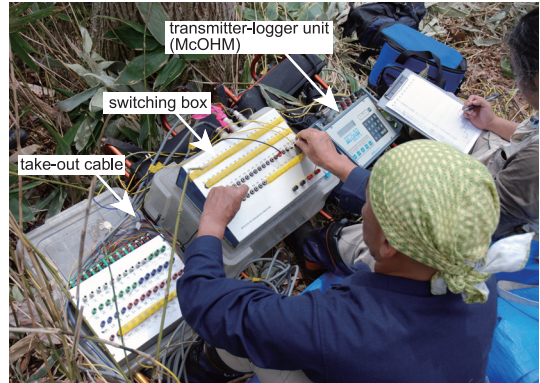


Fig. 5. Photograph of the DC electrical survey in the field using a transmitter-logger unit (McOHM) and a switching box, which is connected to 71 electrodes via take-out cables. The survey involved changing the sites and intervals of the electrodes using the switching box.

Table 1. Specifications of the exploration systems used for the DC electrical (McOHM) and CSAMT surveys (Geo SEM).

| DC electrical survey (McOHM Model-2115) | |
|---|--|
| Output voltage | 400 Vp-p |
| Output current | 1, 2, 5, 10, 20, 50, 100, 200 mA |
| Electric potential | ± 0.6 V, ± 6 V (auto range) |
| Resolution | 20 μ V |
| Cycle time | 3.5 sec |
| Battery | 12 V |
| CSAMT survey (Geo SEM) | |
| Transmitter | |
| Output power | 5 kW (maximum) |
| Output voltage | 1000 V (maximum) |
| Output current | 10 A (maximum) |
| Frequency | 1, 2, 4, 8, 16, 32, 64, 128, 256, 512, 1024, 2048, 4096, 8192 Hz 20, 40, 80, 160, 320, 640, 1280, 2560, 5120 Hz |
| Generator | 6 kW (maximum), 200V AC, 60 Hz, 3 phases |
| Receiver | |
| Frequency | 1, 2, 4, 8, 16, 32, 64, 128, 256, 512, 1024, 2048, 4096, 8192 Hz 20, 40, 80, 160, 320, 640, 1280, 2560, 5120 Hz |
| Channel | 3 or 5 channels |
| Amplification degree | 0.90 dB (10 dB pitch) |
| Wave analysis | stacking, Fourier transform |

further details of the system can be found in Johmori *et al.* (2010).

The transmitter was positioned 3.5 km WNW of the Hiyoriyama Cryptodome, with its 1.1-km-long grounded-wire oriented N35° E (Fig. 1). The receiver stations were distributed along the same survey line as that used for the DC electrical survey (Fig. 1). The distance between the transmitter and receiver stations was 3.5 km. The survey line was 700 m long and was also oriented N35° E (i.e., parallel to the grounded-wire), passing over the summit of the Hiyoriyama Cryptodome (M1–M11; Fig. 3). The 11 receiver stations (M1–M11) were horizontally spaced at regular intervals of 60–70 m, using a transit and GPS.

The CSAMT survey was performed from 22 to 24 May 2011. The transmitter injected 1–8 A electrical currents

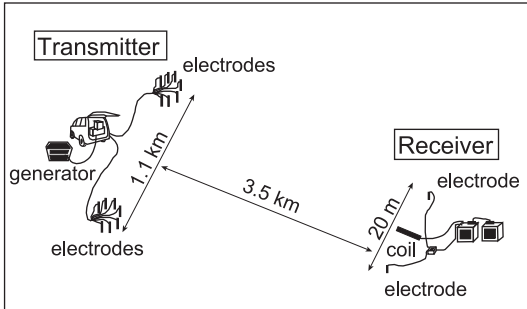


Fig. 6. Schematic of the electromagnetic system (Geo-SEM) used for the CSAMT survey. The grounded-wire for the transmitter is 1.1 km long and has 30 electrodes at each termination. The receiver has sensors consisting of a pair of electrodes and a coil. The distance between the grounded-wire and receiver stations is 3.5 km.

into the ground at frequencies of 1, 2, 4, 8, 16, 32, 64, 128, 256, 512, 1024, 2048, 4096, and 8192 Hz, and another series at frequencies of 20, 40, 80, 160, 320, 640, 1280, 2560, and 5120 Hz, in order to minimize the noise related to the commercially used frequency of 50 Hz and its higher harmonics. The receiver recorded the electric field parallel to the grounded-wire, and the magnetic field perpendicular to the grounded-wire. The measuring time at each receiver station was 1 hour (2 minutes at 8192 Hz, 8 minutes at 1 Hz). The CSAMT data were processed using a band-pass filter and Fourier-transform, to remove noise. The number of sampling waves was $>400,000$ at 8192 Hz or >300 at 1 Hz. The apparent resistivity and phase were then calculated from the electric and magnetic fields. Measurement errors for the apparent resistivity and phase cannot be calculated as the CSAMT data was treated as a single data to maximize the frequency resolution (see Johmori *et al.*, 2010).

Fig. 8 shows the apparent resistivity and phase angles at all receiver stations. The CSAMT data are inferred to have been measured mainly in a far-field region, beyond the near-field region, because (1) the phase angles range from 9° to 30° at 1 Hz (*e.g.*, 20.4° at M5 station, 30° at M6, and 9.3° at M7), with no angles of 0° ; and (2) the apparent resistivity does not show abrupt V-shaped decreasing and increasing trends (*i.e.*, a ‘notch’ or ‘transition zone’; Hishida and Takasugi, 1998) at low frequencies. Below 10 Hz, the apparent resistivity shows a gentle increase with decreasing frequency, whereas the phase angle shows a gentle decrease. This finding may indicate the presence of a high-resistivity body beneath a low-resistivity body, and/or a minor influence on the CSAMT data of the near-field effect. Therefore, it is possible that the CSAMT data are slightly influenced by the near-field effect. Even if this is

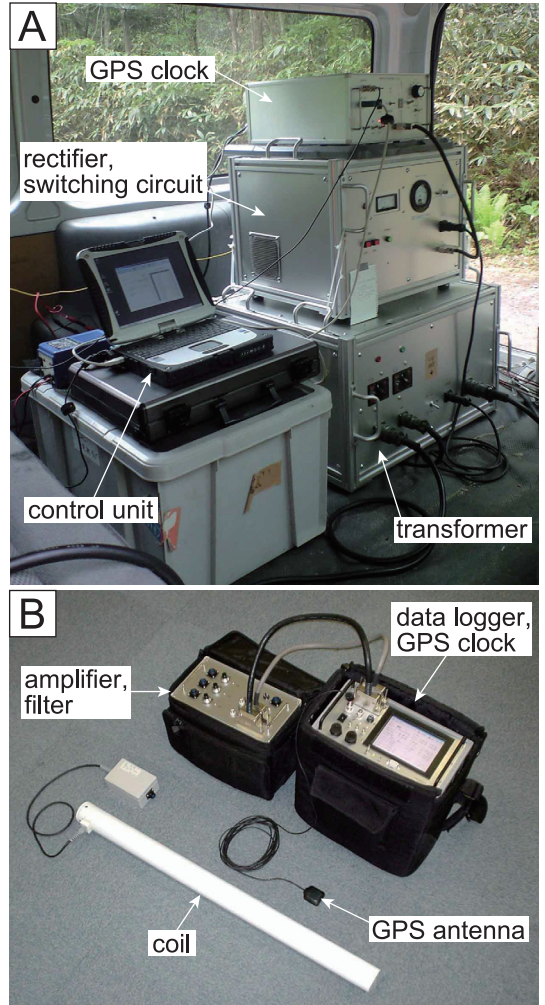


Fig. 7. Photographs of the transmitter (A) and receiver (B) of the electromagnetic system (Geo-SEM) used for the CSAMT survey. The white coil (as shown in B) is 72 cm long.

the case, we infer that the near-field effect has no marked influence on the modeling of resistivity structure at the depths of interest (down to 400 m), given the relation between this depth and the distance between the transmitter and receiver stations (3.5 km, which is 8.8 times larger than the depth of 400 m) (*cf.* Sandberg and Hohmann, 1982).

4. Data analysis

Two-dimensional joint analysis of the DC and CSAMT data was performed to obtain a continuous resistivity structure at depths of up to 400 m beneath the Hiyoriyama Cryptodome. The joint analysis was complicated by the fact that the DC electrical data and the CSAMT data have

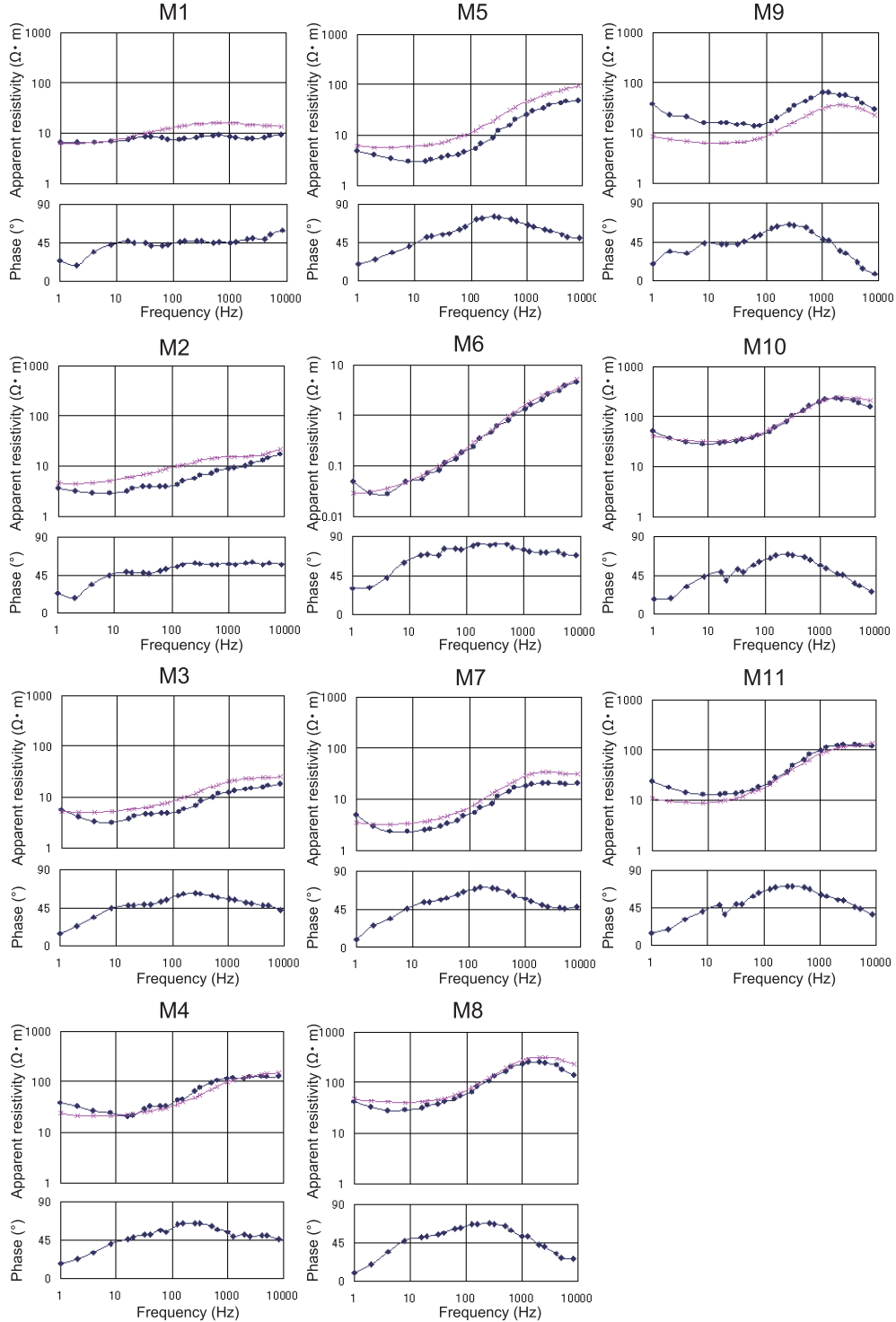


Fig. 8. Apparent resistivity and phase angles of CSAMT field data (blue lines). Calculated results of 2D inversion for the apparent resistivity (RMS=0.08) are also shown (red lines). Location numbers (M1–11) correspond to those shown in Fig. 3.

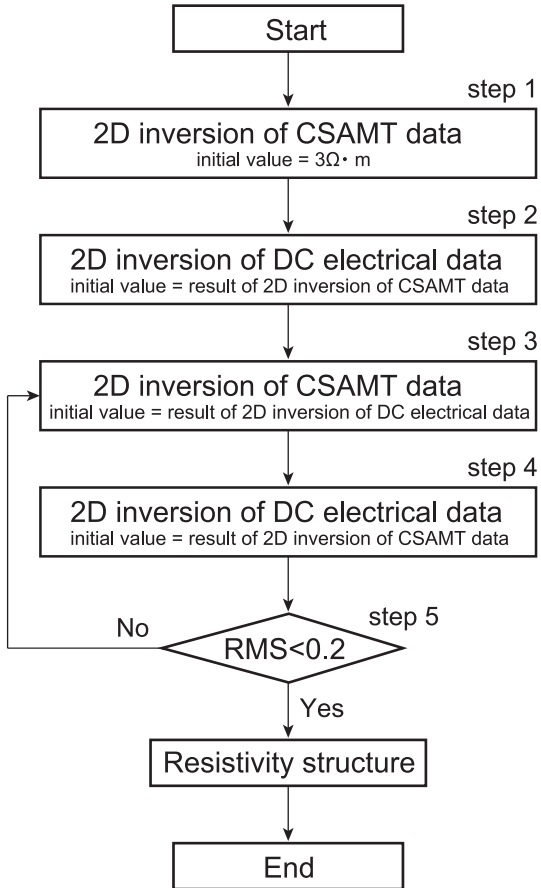


Fig. 9. Flow chart of the procedure for 2D joint inversion of the DC electrical and CSAMT data.

different sensitivities to the three-dimensional structure. In this study, the joint analysis was attempted using seesaw-like calculations of repeated 2D inversions of these data (Fig. 9).

The analytical methods applied to the DC electrical data and the CSAMT data were taken from Sasaki (1981) and Sasaki (1986), respectively. The algorithm of Sasaki (1981) is a 2D inversion using a finite element method for DC electrical surveys, whereas the algorithm of Sasaki (1986) is a 2D inversion using a finite element method for MT surveys. The mesh size of the finite element method for DC data analysis was 5 m (element size, 5×5 m), while that for CSAMT data analysis was 10 m (element size, 10×10 m). Each inversion block (i.e., the unit used to calculate resistivity by 2D inversion; Sasaki, 1986) consisted of four elements. In the joint analysis, the 5-m-mesh DC resistivity data were interpolated and used as an initial model for the 10-m-mesh CSAMT data analysis; conversely, the 10-m-mesh CSAMT data were interpolated and used as an initial model for the 5-m-mesh DC data

analysis.

While the CSAMT data consisted of apparent resistivity and phase angles, the 2D inversions were performed using the apparent resistivity only (cf. Sasaki, 1986). Phase angles were not used in the 2D inversions. Static shift for the CSAMT data was reduced by the 2D inversions. Even if a near-surface resistivity-anomaly was present, it was detected by the DC electrical data and incorporated into the CSAMT analytical model. Topographic effects for the DC and CSAMT data were reduced by the 2D inversions. High-resolution, aerial, laser-scanner mapping data (Goto *et al.*, 2011a) were used to produce topographic models for the 2D inversions.

The calculation process involved the following five steps (Fig. 9). (1) A resistivity structure was calculated by 2D inversion of the CSAMT data, setting a uniform resistivity ($3\Omega \cdot m$) as the initial model. The value of $3\Omega \cdot m$ was based on the very low resistivity in the Noboribetsu Geothermal Field (Goto and Johmori, 2011). (2) A resistivity structure was calculated by 2D inversion of the DC electrical data, setting the result of the 2D inversion of the CSAMT data as the initial model. (3) A resistivity structure was calculated by 2D inversion of the CSAMT data, setting the result of the 2D inversion of the DC electrical data as the initial model. (4) A resistivity structure was calculated by 2D inversion of the DC electrical data, setting the result of the 2D inversion of the CSAMT data as the initial model. (5) Root mean square (RMS) values were calculated from the field data and from the results of steps (3) and (4). The RMS value (δ) is defined as $\delta = [\sum \{\ln(\rho_{af}) - \ln(\rho_{ac})\}^2 / n]^{1/2}$, where ρ_{af} is the field measurement (apparent resistivity) and ρ_{ac} is the calculated result. An RMS value equal to zero means that the calculated result perfectly matches the field data. RMS values were calculated separately for the CSAMT data and the DC electrical data.

If the RMS values exceeded 0.2, steps (3) and (4) were repeated. If the RMS values were lower than 0.2, the calculated result was accepted as the resistivity that satisfies both the CSAMT and DC electrical data. In this study, steps (3) and (4) were repeated four times, yielding RMS values of 0.08 (at step 3) and 0.19 (at step 4). Fig. 10A and B shows the calculated results of 2D joint inversion when steps (3) and (4) were repeated three times (RMS = 0.09 at step 3; RMS = 0.26 at step 4), whereas Fig. 10C and D shows the calculated results when steps (3) and (4) were repeated four times (RMS = 0.08 at step 3, RMS = 0.19 at step 4). Fig. 8 compares the CSAMT field data (apparent resistivity) with the calculated result at step (3) (RMS = 0.08), while Fig. 11 compares the DC electrical field data (apparent resistivity) with the calculated result at step (4) (RMS = 0.19).

Before accepting the calculated result (Fig. 10D), we tested an alternative 2D joint analysis, employing both apparent resistivity and phase angles in the algorithm of

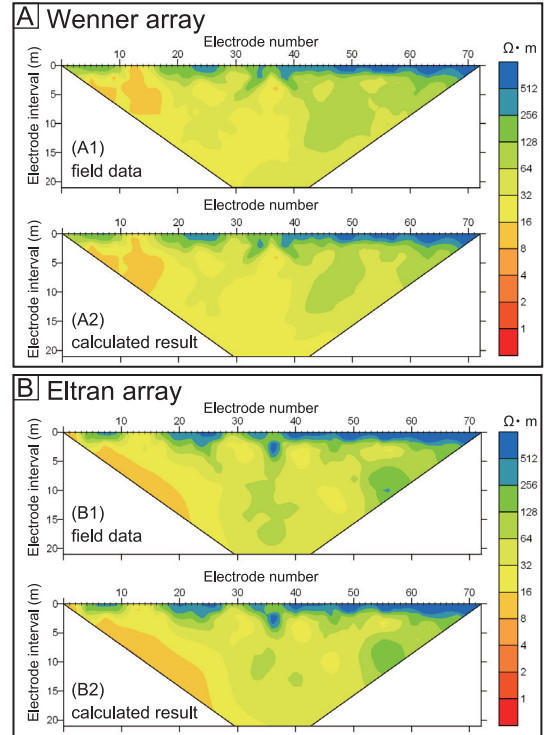
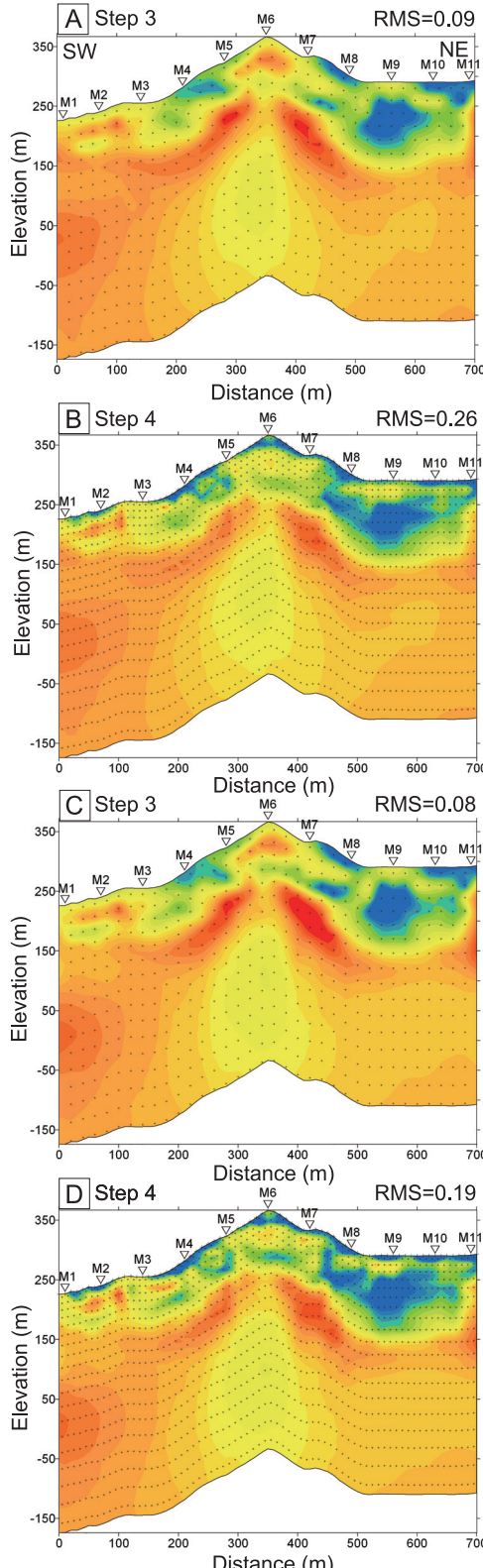


Fig. 11. Comparison of the DC electrical field data (apparent resistivity; A1: Wenner array; B1: Eltran array) and calculated results of the 2D inversion (A2: Wenner array; B2: Eltran array) ($\text{RMS}=0.19$).

Fig. 10. Process of 2D joint inversion of the DC electrical and CSAMT data. (A) and (B) Calculated results of 2D joint inversion for three repetitions of steps (3) and (4) (see Fig. 9) ($\text{RMS}=0.09$ at step 3; $\text{RMS}=0.26$ at step 4). (C) and (D) Calculated results of 2D joint inversion for four repetitions of steps (3) and (4) ($\text{RMS}=0.08$ at step 3, $\text{RMS}=0.19$ at step 4). Small dots in (A)–(D) indicate the distributions of the centers of inversion blocks.

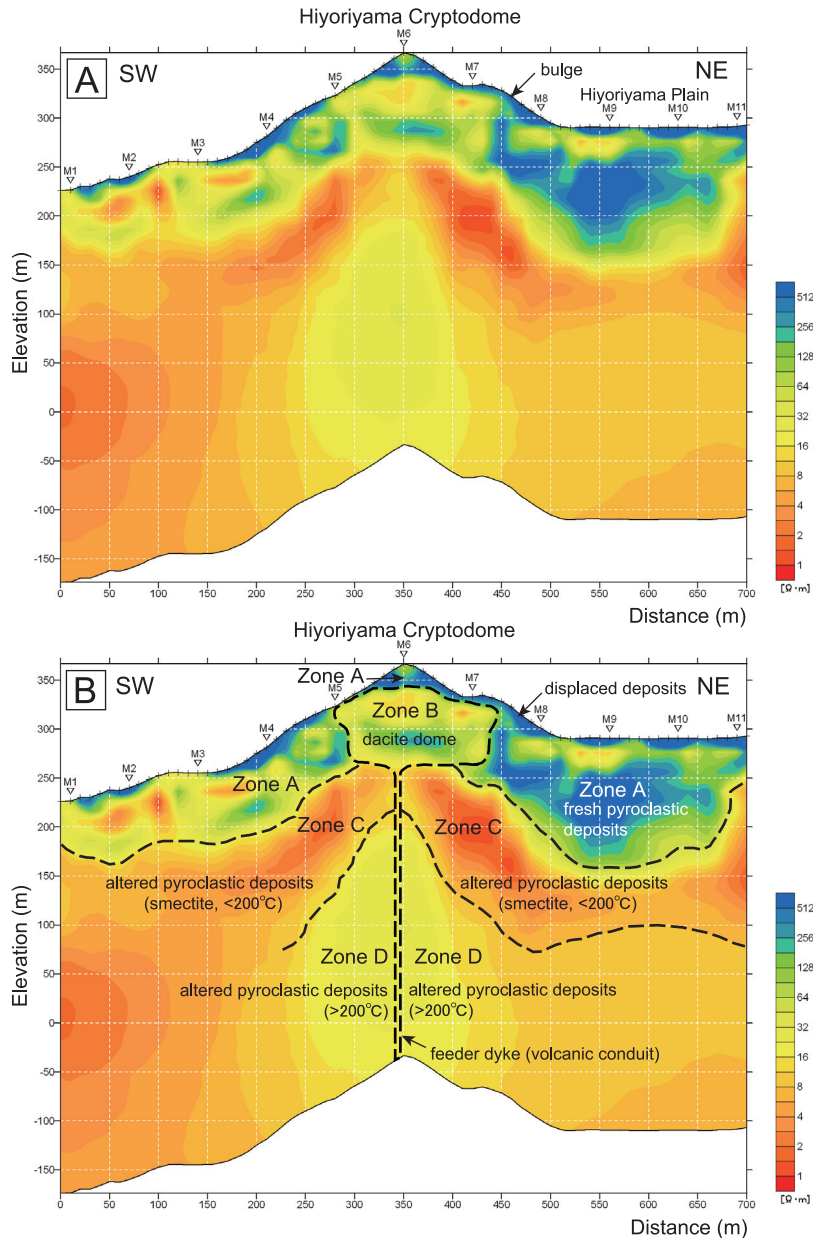


Fig. 12. Resistivity section beneath the Hiyoriyama Cryptodome (A) and its geological interpretation (B). Zone A is interpreted to represent fresh (unaltered) pyroclastic deposits erupted from Kuttara Volcano. Zone A at the Hiyoriyama Cryptodome (10–30 m thick; above zone B) is interpreted to be pyroclastic deposits uplifted by growth of the cryptodome. Zone B (150 m wide, 80 m thick) is interpreted as the dacite intrusion of the cryptodome. Zone C is interpreted as altered pyroclastic deposits containing abundant conductive clay minerals, such as smectite, formed by low-temperature ($<200^{\circ}\text{C}$) hydrothermal alteration in the region between the cold ground surface and deeper, hotter regions. Zone D is interpreted as altered pyroclastic deposits that have been subjected to higher-temperature ($>200^{\circ}\text{C}$) hydrothermal alteration in a deeper, hotter region near the conduit of the Hiyoriyama Cryptodome. The location of the feeder dyke is estimated from the topographic features of the Hiyoriyama Cryptodome.

Sasaki (1986). This calculation resulted in a reduced degree of convergence compared with the 2D joint analysis using apparent resistivity only; steps (3) and (4) were repeated four times, yielding RMS values of 0.19 (at step 3) and 0.19 (at step 4). The reduced degree of convergence could be attributed to data dispersion in the phase angles (see Fig. 8). The obtained resistivity structure was almost identical to that using apparent resistivity only, but was slightly more irregular. In this study, we placed greater emphasis on the degree of convergence rather than phase angles, and adopted the resistivity structure obtained using apparent resistivity only (Fig. 10D) as the final model.

The depth of penetration was determined from the skin depth (Cagniard, 1953) and the Bostick depth (Murakami, 1987). The skin depth is defined as the depth at which the amplitude of electromagnetic waves decrease to $1/e$ (e is the base of the natural logarithm). The Bostick depth is defined as $1/\sqrt{2}$ of the skin depth, and is considered to represent a more accurate depth of penetration than the skin depth. The skin depth calculated from the frequency of electric currents for the deepest layer (1 Hz) and from its apparent resistivity ($3\text{--}5 \Omega \cdot \text{m}$) for the CSAMT data, yields a penetration depth of 866–1120 m, whereas the Bostick depth calculated from the same data yields a penetration depth of 612–792 m. Given that the topography along the survey line varies in elevation from 225 to 350 m and has relatively steep slopes, we conservatively estimate the depth of penetration to be about 400 m below the ground surface.

5. Results and discussion

Processing of the DC electrical and CSAMT data revealed the subsurface resistivity structure at depths of less than 400 m beneath the Hiyoriyama Cryptodome (Fig. 12A). The resistivity structure is divided into four zones based on the resistivity values (A–D in Fig. 12B). In general, the resistivity of rocks and sediments is lowered by the presence of conductive minerals (*e.g.*, smectite-series clays), thermal water in pores and fractures, and high temperatures (*e.g.*, Risk *et al.*, 2003). Geological interpretations of the four zones (A–D in Fig. 12B) are provided as follows.

Zone A (resistivity of $> 100 \Omega \cdot \text{m}$) extends subhorizontally along the ground surface and is ~ 100 m thick beneath the Hiyoriyama Plain, and 10–30 m thick at the Hiyoriyama Cryptodome. Because the surface geology in this area consists of pyroclastic deposits erupted from Kuttara Volcano at *ca.* 40 ka (mainly the Kt-1 pyroclastic flow deposit), zone A is interpreted to represent these deposits. The high resistivity of this zone suggests that the deposits are fresh and unaltered. Zone A at the Hiyoriyama Cryptodome (10–30 m thick; above zone B) is interpreted to be pyroclastic deposits uplifted by growth of the cryptodome.

Zone B ($20\text{--}50 \Omega \cdot \text{m}$) is located below the Hiyoriyama

Cryptodome and occupies a semi-rectangular domain that is 150 m wide and 80 m thick in cross-section. Given that zone B is located immediately beneath the cryptodome, we interpret this zone as the dacite intrusion of the cryptodome. Considering the emplacement age of the Hiyoriyama Cryptodome (*ca.* 15 ka; Goto and Danhara, 2011), the dacite intrusion is probably solidified. The intermediate resistivity ($20\text{--}50 \Omega \cdot \text{m}$) is explained by hydrothermal alteration of solidified dacite. The bulge at the northeastern slope of the cryptodome (Fig. 12A) reflects lateral displacement of the pyroclastic deposits that resulted from emplacement of the dacite intrusion during growth of the cryptodome (displaced deposits; Fig. 12B).

Zone C occurs 100–200 m below the cryptodome and is characterized by very low resistivity ($< 5 \Omega \cdot \text{m}$). This zone is ~ 100 m thick, convex-shaped, and is conspicuous in the resistivity section. The convex shape is symmetrical with respect to a vertical line passing through the summit of the cryptodome. The top of the convex body appears to fade out, with the zone being discontinuous at the vertical line. Possible interpretations of zone C include: (1) altered pyroclastic deposits containing abundant conductive clay minerals, such as smectite; (2) pyroclastic deposits containing thermal water in pores and fractures; and (3) high-temperature pyroclastic deposits. We favor interpretation (1) because interpretations (2) and (3) cannot readily explain the convex geometry of the zone. We infer that the convex-shaped geometry reflects the distribution of the stability field of smectite ($< 200^\circ\text{C}$; Hyndman *et al.*, 1997; Aizawa *et al.*, 2009; Aizawa, 2010; Lee *et al.*, 2010). The fade-out at the top of the convex body could be attributed to the instability of smectite (which occurs at temperatures of $> 200^\circ\text{C}$) due to the ascent of high-temperature fluids along the feeder dyke beneath the dome. Zone C is therefore interpreted as altered pyroclastic deposits subjected to low-temperature ($< 200^\circ\text{C}$) hydrothermal alteration in the region between the cold ground surface and deeper, hotter regions. Zone C is rich in clay minerals and may form an impermeable ‘sealing zone’ (Aizawa *et al.*, 2009; Aizawa, 2010) below fresh, permeable pyroclastic deposits (zone A).

Zone D occurs beneath zone C (150–400 m below the ground surface) and shows higher resistivity ($10\text{--}30 \Omega \cdot \text{m}$). The oval shape of zone D remains uncertain, as the resistivity resolution at this depth is insufficient to reliably constrain its outline. A possible interpretation of zone D is altered pyroclastic deposits containing fewer conductive clay minerals than in zone C (*e.g.*, it may contain chlorite rather than smectite). The higher resistivity can potentially be attributed to the higher temperature of the zone, which means that smectite is unstable ($> 200^\circ\text{C}$). A higher temperature is plausible because zone D is deeper than zone C, and located closer to the inferred feeder dyke of the dome. Zone D is therefore interpreted as altered pyroclastic deposits that have been subjected to higher-

temperature ($>200^{\circ}\text{C}$) hydrothermal alteration in a deeper, hotter region near the conduit of the Hiyoriyama Cryptodome.

6. Conclusions

DC electrical and CSAMT surveys have revealed the subsurface resistivity structure at depths shallower than 400 m beneath the Hiyoriyama Cryptodome. The resistivity structure suggests that the cryptodome comprises a dacite intrusion (150 m wide, 80 m thick) and overlying pyroclastic deposits (10–30 m thick). The dacite intrusion is underlain by hydrothermally altered pyroclastic deposits (>300 m) that are divided into two zones based on the assemblage of alteration minerals. The upper zone contains abundant conductive clay minerals such as smectite that formed by low-temperature alteration, whereas the lower zone contains fewer conductive clay minerals and formed by higher-temperature alteration in a deeper, hotter region near the conduit of the cryptodome.

Acknowledgments

This research was sponsored by the Ministry of Education, Culture, Sports, Science and Technology of Japan (MEXT), and was financially supported by the Muroran Institute of Technology. We thank N. Johmori, T. Kondou and T. Takahashi (Neo Science Co. Ltd) for help in the field. S. Kameyama (Tanaka Consultant Co. Ltd) is thanked for providing topographic data for the Hiyoriyama Cryptodome. Comments by K. Aizawa (University of Tokyo), an anonymous referee and T. Watanabe (University of Toyama) significantly improved the manuscript.

References

- Aizawa, K. (2010) Groundwater flow beneath volcanoes inferred from electric self-potential and magnetotellurics. *Bull. Volcanol. Soc. Japan*, **55**, 251–259. (in Japanese)
- Aizawa, K., Ogawa, Y., Hashimoto, T., Koyama, T., Kanda, W., Yamaya, Y., Mishina, M. and Kagiya, T. (2008) Shallow resistivity structure of Asama volcano and its implications for magma ascent process in the 2004 eruption. *J. Volcanol. Geotherm. Res.* **173**, 165–177.
- Aizawa, K., Ogawa, Y. and Ishido, T. (2009) Groundwater flow and hydrothermal systems within volcanic edifices: Delination by electric self-potential and magnetotellurics. *J. Geophys. Res.*, **114**, doi: B0120810.1029/2008jb005910.
- Cagniard, I. (1953) Basic theory of the magnetotelluric method of geophysical prospecting. *Geophysics*, **18**, 605–635.
- Goto, Y. and Danhara, T. (2011) Zircon fission-track dating of the Hiyoriyama Cryptodome at Kuttara Volcano, southwestern Hokkaido, Japan. *Bull. Volcanol. Soc. Japan*, **56**, 19–23.
- Goto, Y. and Johmori, A. (2011) Controlled source audio-frequency magnetotelluric (CSAMT) and time domain electromagnetic (TDEM) resistivity measurements at Noboribetsu Geothermal Field, Kuttara Volcano, Hokkaido, Japan. *Bull. Volcanol. Soc. Japan*, **56**, 153–160.
- Goto, Y., Matsuzuka, S. and Kameyama, S. (2011a) Three-dimensional digital mapping of Noboribetsu Geothermal Field, Kuttara Volcano, Hokkaido, Japan, using helicopter-borne high-resolution laser scanner. *Bull. Volcanol. Soc. Japan*, **56**, 127–135.
- Goto, Y., Sasaki, H., Toriguchi, Y. and Hatakeyama, A. (2011b) Phreatic explosion after AD 1663 at the Hiyoriyama Cryptodome, Kuttara Volcano, southwestern Hokkaido, Japan. *Bull. Volcanol. Soc. Japan*, **56**, 147–152.
- Hishida, H. and Takasugi, S. (1998) The CSAMT method. In *Handbook for geophysical exploration* (Society of Exploration Geophysics of Japan ed.), 322–325, Society of Exploration Geophysics of Japan. (in Japanese)
- Hyndman, R.D., Yamano, M. and Oleskevich, D.A. (1997) The seismogenic zone of subduction thrust faults. *Island Arc*, **6**, 244–260.
- Johmori, A., Mitsuhasha, Y., Nishimura, S., Johmori, N., Kondou, T. and Takahashi, T. (2010) Development of a deep electromagnetic exploration instrument with high frequency spectrum resolution using GPS synchronization. *Jour. Japan Soc. Engin. Geol.*, **51**, 62–72. (in Japanese with English abstract)
- Katsui, Y., Yokoyama, I., Okada, H., Abiko, T. and Muto, H. (1988) *Kuttara (Hiyoriyama), its volcanic geology, history of eruption, present state of activity and prevention of disasters*. Committee for Prevention and Disasters of Hokkaido, Sapporo, 99p. (in Japanese)
- Lee, J.O., Kang, I.M. and Cho, W.J. (2010) Smectite alteration and its influence of the barrier properties of smectite clay for a repository. *Applied Clay Science*, **47**, 99–104.
- Matsuoka, T. (2005) *Dictionary of exploration geophysics*. Society of Exploration Geophysics of Japan ed., Aichi Shuppan, Tokyo, 279p. (in Japanese)
- Milsom, J. (2003) *Field Geophysics*. John Wiley and Sons, Ltd, England, 232p.
- Moriizumi, M. (1998) The growth history of the Kuttara volcanic group. *Bull. Volcanol. Soc. Japan*, **43**, 95–111. (in Japanese with English abstract)
- Moriya, I. (2003) Kuttara Volcano. In *Regional Geomorphology of the Japanese Islands, vol. 2, Geomorphology of Hokkaido* (Koaze T., Nogami, M., Ono, Y. and Hirakawa, K. eds.), 279–281, University of Tokyo Press, Tokyo. (in Japanese)
- Murakami, Y. (1987) Bostic inversion. *Butsuri-Tansa*, **40**, 282–291.
- NEDO (New Energy and Industrial Technology Development Organization) (1991) *Noboribetsu, Report of promotional exploration for geothermal research*, No. 22. NEDO, Tokyo, 845p. (in Japanese)
- Risk, G.F., Caldwell, T.G. and Bibby, H.M. (2003) Tensor time domain electromagnetic resistivity measurements at Ngatamariki geothermal field, New Zealand. *J. Volcanol. Geotherm. Res.* **127**, 33–54.
- Sandberg, S. and Hohmann, G. (1982) Controlled-source audio-magnetotellurics in geothermal exploration. *Geophysics*, **47**,

- 100–116.
- Sasaki, Y. (1981) Automatic interpretation of resistivity sounding data over two-dimensional structures (I). *Geophysical Exploration*, **34**, 15–24.
- Sasaki, Y. (1986) Resolving power of MT method for two-dimensional structures. *Geophysical Exploration*, **39**, 1–9.
- Srigutomo, W., Kagiyama, T., Kanda, W., Munekane, H., Hashimoto, T., Tanaka, Y., Utada, H. and Utsugi, M. (2008) Resistivity structure of Unzen volcano derived from time domain electromagnetic (TDEM) survey. *J. Volcanol. Geotherm. Res.* **175**, 231–240.
- Yamagata, K. (1994) Tephrochronological study on the Shikotsu and Kuttara Volcanoes in southwestern Hokkaido, Japan. *J. Geogr.*, **103**, 268–285. (in Japanese with English abstract)
- (Editorial handling Toru Watanabe)

北海道南西部クッタラ火山、日和山潜在ドームの比抵抗構造

後藤芳彦・城森 明

北海道南西部クッタラ火山、日和山潜在ドームの比抵抗構造探査を行い、日和山潜在ドームの内部構造（深度<400 m）を解明した。探査は高密度電気探査法およびCSAMT 探査法を用い、ドームを北東–南西方向に横断する測線上で行った。測線長は700 mで、受信点は高密度電気探査 71 電極、CSAMT 探査 11 測点を等間隔に配置した。データ解析は高密度電気探査およびCSAMT 探査データの2D ジョイント解析を行った。日和山潜在ドームは、幅150 m 高さ80 m のデイサイト貫入岩体(20–50 $\Omega \cdot m$)と、貫入岩体を覆う厚さ10–30 m の火碎堆積物(>100 $\Omega \cdot m$)からなる。デイサイト貫入岩体の直下には、ハの字型の低比抵抗領域(<10 $\Omega \cdot m$)が存在し、スメクタイトに富む低温(<200°C)の熱水変質帶であると考えられる。この低比抵抗領域の直下には中比抵抗領域(10–30 $\Omega \cdot m$)が存在し、ドームの供給岩脈(火道)に沿って形成された高温(>200°C)の熱水変質帶であると考えられる。